LCLS-II-HE emittance with sextupoles

LCLS-II-HE-TN-23-02

5/19/2023

Y. Nosochkov and T. Raubenheimer, SLAC

1 Introduction

To guide the LCLS-II-HE beam in the tunnel, horizontal and/or vertical bending magnets are included at various locations of the beamline. The main sections where the trajectory changes occur are the bypass dogleg, the HXR and SXR beam spreader lines, and the HXR and SXR LTU doglegs. The bending creates momentum dispersion which together with the beam energy spread can lead to emittance growth, if not promptly cancelled. In the nominal design, the first order dispersion is locally cancelled in each of the bending sections using an appropriate quadrupole focusing between the dipoles. The residual second order dispersion, however, still creates emittance growth according to [1]:

$$\frac{\Delta\varepsilon}{\varepsilon_0} = \frac{2}{5}\frac{1}{\beta\varepsilon_0}[\eta_2^2 + (\alpha\eta_2 + \beta\eta_2')^2]\sigma_\delta^4 \qquad (1)$$

where ε_0 is the initial un-normalized emittance (without γ); η_2, η_2' are the second order spatial and angular dispersion measured at a point soon after the bending section; α and β are the Twiss functions at the same point; and σ_δ is the beam rms energy spread, assuming flat energy distribution in this formula.

Emittance growth in Eq. (1) can be significant at large σ_δ, e.g. in beam conditions with large chirp. To compensate this effect, the LCLS-II-HE reserves space for two sextupoles per each bending section for local cancellation of the second order dispersion, except the HXR LTU dogleg where the residual non-linear dispersion is small. With the second order dispersion corrected, the remaining emittance growth is due to the higher order dispersion which becomes important only for very large energy spread. Schematic of the LCLS-II-HE layout with the sextupole locations is presented in Figure 1. Linear optics of the individual bending sections with the reserved sextupoles are shown in Figure 2 and Figure 3. The sextupole locations in each section are selected based on the appropriate phase advance and optics functions at the two sextupoles for efficient correction and reasonable sextupole strengths.

While the sextupoles eliminate emittance growth caused by the second order dispersion, they create another source of emittance growth through unavoidable sextupole alignment errors. It is therefore important to verify if the sextupole correction still provides significant emittance compensation when sextupole misalignment is taken into account. This can be done by comparing the emittance growth in two cases: 1) without sextupoles, and 2) with the sextupole correction and realistic sextupole misalignment. In this paper, we first quantify the emittance growth due to the second order dispersion with and without sextupole correction; then we evaluate this effect with the correction and sextupole misalignment. Based on these results, one can decide whether the sextupoles are cost-effective for emittance control in the LCLS-II-HE. Optics calculations are performed using MAD [2], while emittance is calculated in tracking simulations using `elegant` [3]; the latter are compared to analytic estimates. The results are for the LCLS-II-HE lattice version of July 04, 2020 [4].

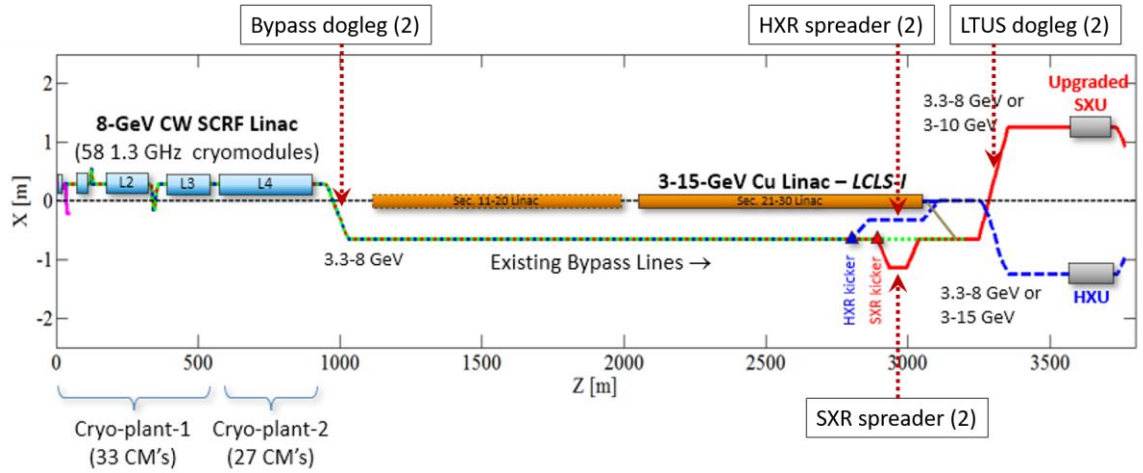

Figure 1: Schematic of the LCLS-II-HE layout (top view). Areas of the sextupole locations are indicated by the arrows; the number of the sextupoles is shown in brackets.

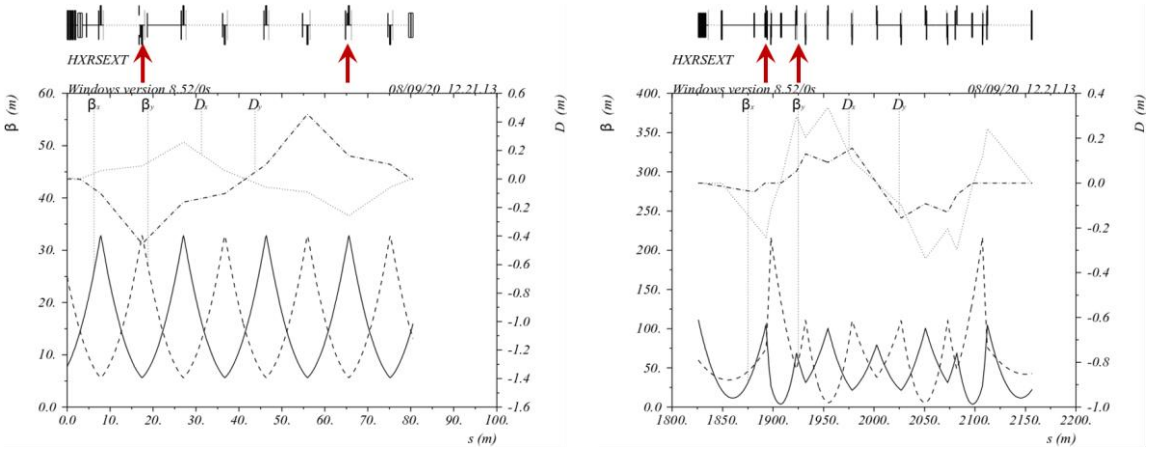

Figure 2: Left – HXR/SXR bypass dogleg optics and locations of sextupoles SDOG1, SDOG2 (shown by arrows); Right – HXR spreader optics and locations of sextupoles SSP1H, SSP2H.

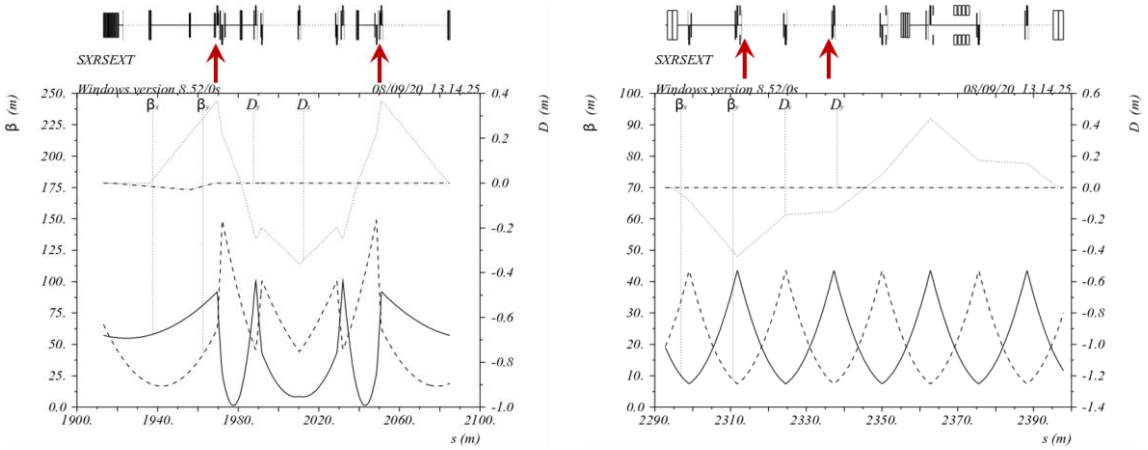

Figure 3: Left – SXR spreader optics and locations of sextupoles SSP1S, SSP2S (shown by arrows); Right – SXR LTU dogleg optics and locations of sextupoles SDL1, SDL2.

2 Second order dispersion and emittance growth

2.1 Second order dispersion

The eight sextupoles considered for the LCLS-II-HE include the HXR/SXR shared sextupoles SDOG1, SDOG2 in the bypass dogleg, the SSP1H, SSP2H sextupoles in the HXR spreader line, the SSP1S, SSP2S sextupoles in the SXR spreader line, and the SDL1, SDL2 sextupoles in the SXR LTU dogleg. The beam in the bypass dogleg and the HXR spreader is deflected both horizontally and vertically. The created horizontal (x) and vertical (y) second order dispersion is locally cancelled in each section using the corresponding two rolled sextupoles by matching the sextupole K_2 values and the roll angles. Bending in the SXR spreader and the SXR LTU dogleg is primarily horizontal yielding a horizontal second order dispersion. The latter is cancelled using two normal sextupoles in each section by matching the sextupole K_2 values.

When all the eight sextupoles are used, the second order dispersion is locally cancelled within each section as shown in Figure 4. There are three areas in this Figure, near S = 0, 2000 m and 2300 m, where the second

order dispersion bumps can be seen. These correspond to the bypass dogleg, the HXR/SXR spreader, and the LTU doglegs. Due to the very small second order dispersion in the HXR LTU dogleg, sextupoles are not needed there. Note that the vertical scale in Figure 4 is chosen to be the same as in the next Figures showing uncompensated second order dispersion, for easier comparison.

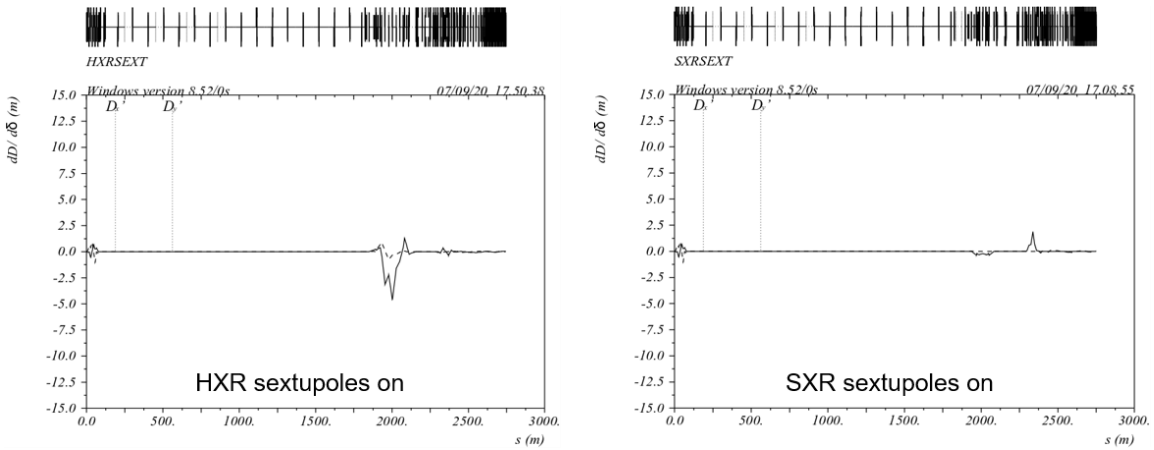

Figure 4: Second order dispersion in HXR (left) and SXR (right) beamlines from bypass dogleg to the main dumps with all sextupoles turned on.

The second order dispersion with the sextupoles turned off in one of the bending sections is shown in Figure 5 and Figure 6. The second order dispersion leaking out of the uncompensated section performs free betatron oscillations along the beamline with an amplitude scaled as $\sqrt{\beta}$. It can be seen in Figure 5 that the uncorrected second order dispersion from the bypass dogleg is predominantly vertical, thus affecting more the vertical emittance in both HXR and SXR, while in the HXR spreader it is mostly horizontal affecting the horizontal emittance. Bending in the SXR spreader and the SXR LTU is primarily horizontal, hence the corresponding emittance growth is in the horizontal plane.

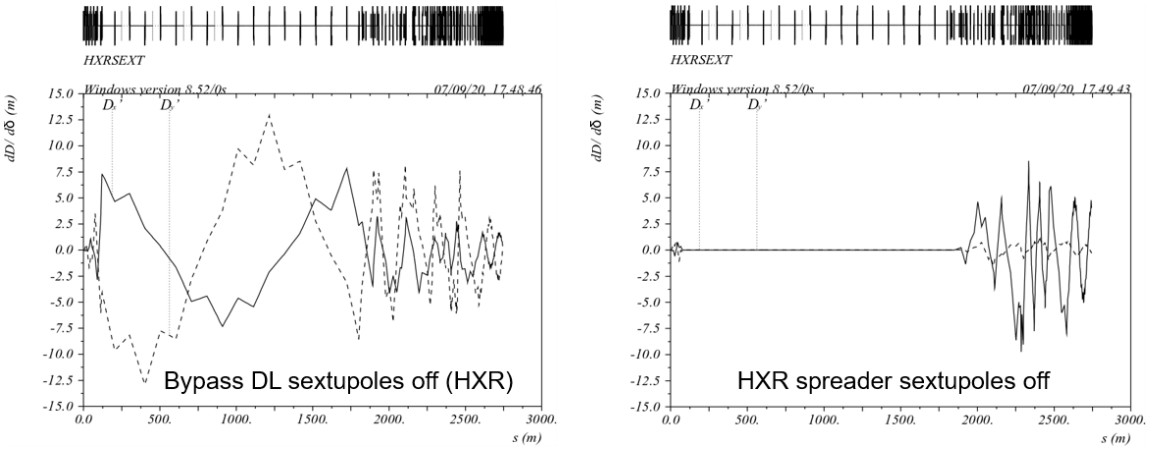

Figure 5: HXR second order dispersion with the sextupoles turned on except the bypass dogleg sextupoles (left), or the HXR spreader sextupoles (right). The second order dispersion without the bypass dogleg sextupoles is identical in the HXR and SXR up to the beginning of the spreader.

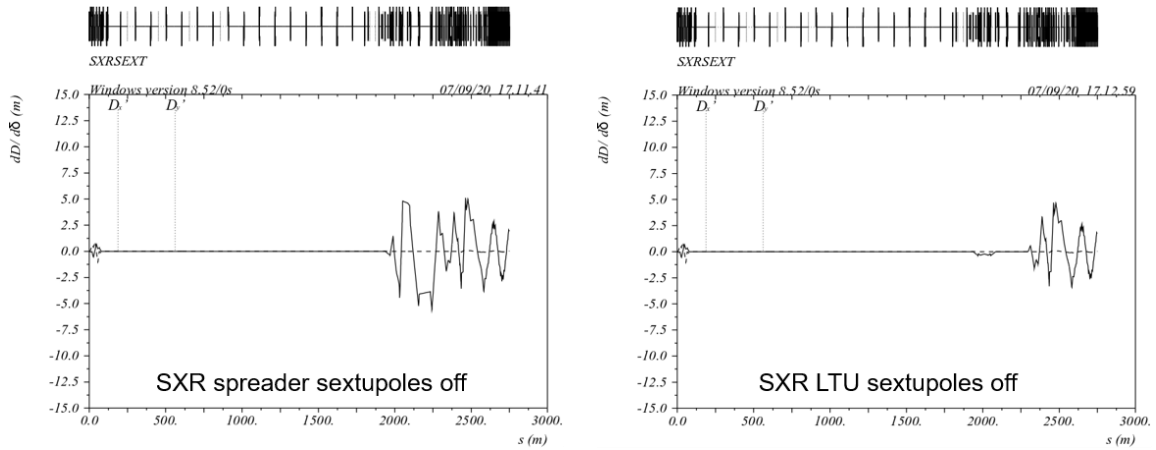

Figure 6: SXR second order dispersion with the sextupoles turned on except the SXR spreader sextupoles (left), or the SXR LTU dogleg sextupoles (right).

2.2 Emittance growth

Effect of the second and higher order dispersion on emittance with and without the LCLS-II-HE sextupoles is evaluated using tracking simulations in `elegant` where the studied HXR and SXR beamlines begin at entrance of the first dipole in the bypass dogleg and end at the beginning of the corresponding undulator. Only the optics effects are included in the simulations, thus excluding the incoherent and coherent synchrotron radiation and the space charge. Ideal magnets are considered except when studying the sextupole misalignment. The initial beam of 10^5 electrons is randomly generated based on the following parameters: 8 GeV average energy; Gaussian distribution in *x-y* space with normalized emittance of $\gamma\varepsilon_{x0}$ = 0.52 μm and $\gamma\varepsilon_{y0}$ = 0.42 μm; nominal Twiss functions at the beginning of the bypass dogleg of β_x = 7.7813 m, β_y = 24.8542 m, α_x = -0.8008, α_y = 2.0167; rms bunch length of 9 μm; and uniform (flat) energy distribution with σ_δ being the rms of relative momentum deviation. The initial emittance values are taken from the realistic start-to-end tracking simulations by J. Qiang [5].

HXR and SXR normalized emittance at end of the beamlines as a function of rms energy spread with all the sextupoles turned on are shown in Figure 7. In this case, the second order dispersion is cancelled within each bending section, so the remaining effect is due to higher order dispersion. The resulting emittance growth is negligible at typical beam energy spread of $\sigma_\delta \approx 0.1\%$ and still small at up to $\sigma_\delta \approx 0.5\%$. At larger σ_δ the emittance exhibits fast growth leading to large beam size and eventual particle loss at collimators at $\sigma_\delta >$ 1.1%. After the lost electrons with large amplitudes are removed from the tracked beam by the collimators, their large contribution to emittance is also removed causing the subsequent rate of emittance growth to be reduced as can be seen in Figure 7 plots.

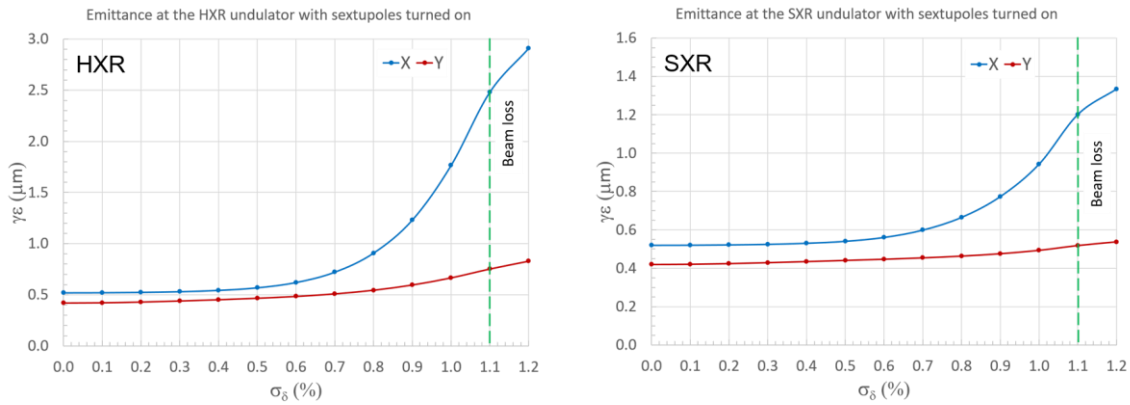

Figure 7: HXR (left) and SXR (right) emittance at the beginning of undulators vs rms energy spread with all sextupoles turned on. Enlargement of beam size leads to beam loss at collimators at σ_δ > 1.1%.

An example where a large emittance growth caused by large σ_δ results in particle loss is presented in Figure 8. It shows the vertical beam distribution and energy spread at the energy collimator CEDOG inside the bypass dogleg with the sextupoles turned on. The collimator vertical aperture is ±8.6 mm; due to the linear and higher order dispersion the full vertical beam spread reaches the size of the collimator aperture at about σ_δ = 1.1%. For a flat energy distribution this corresponds to a full energy spread of $\delta = \pm\sqrt{3}\sigma_\delta \approx \pm 1.9\%$. Since the beam size is dominated by dispersion, the vertical distribution is also nearly flat. At $\sigma_\delta > 1.1\%$ the beam size exceeds the collimator aperture resulting in particle loss.

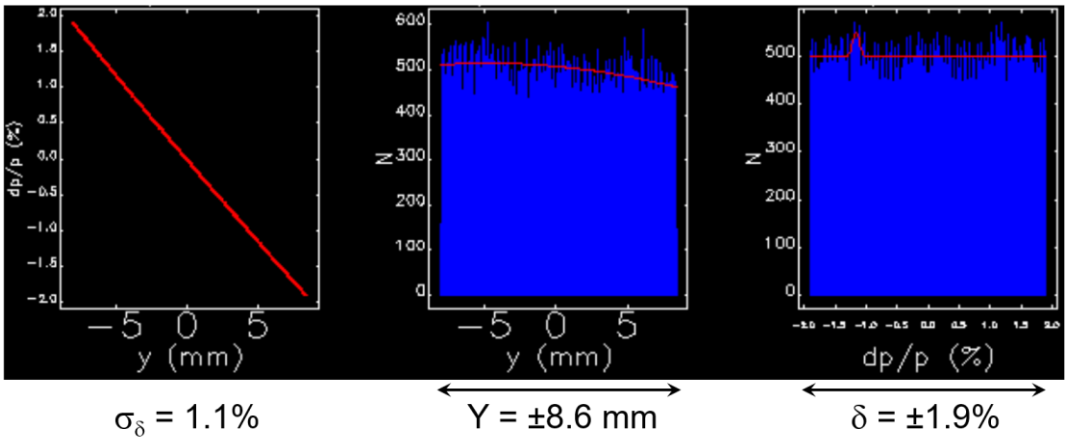

Figure 8: Example of beam distribution at CEDOG energy collimator in the bypass dogleg at σ_δ = 1.1% with sextupoles turned on. At this large σ_δ the beam vertical spread completely fills the collimator vertical aperture of ±8.6 mm. Beam loss on the CEDOG occurs at σ_δ > 1.1%.

Without the sextupole correction, the second order dispersion can cause significant emittance growth. This is demonstrated in Figure 9 and Figure 10, where the sextupoles are turned off in one of the bending sections. The SXR emittance with bypass dogleg sextupoles turned off is not shown as it is quantitatively similar to the corresponding HXR plot.

The missing sextupole correction even in one section results in more than ten-fold increase in emittance at large σ_δ relative to emittance with complete sextupole correction. Without the correction, the range of energy spread where the impact on emittance is relatively small is reduced to $\sigma_\delta \leq 0.2\%$. The plotted range in Figure 9 and Figure 10 is limited to maximum σ_δ where there is no beam loss on collimators. Comparison with Figure 7 shows that σ_δ threshold at which losses start to occur is reduced by as much as 35% without sextupoles in one of the sections as compared to the case with all sextupoles, thus potentially limiting operation scenarios with high chirp. One can also notice that large vertical emittance occurs only due to missing sextupoles in the bypass dogleg. Missing sextupoles in other sections can result in large horizontal emittance, but have small impact on the vertical emittance.

The effect of emittance growth on beam size enlargement at small and large σ_δ with the bypass dogleg sextupoles turned off is demonstrated in Figure 11. The beam size growth can be most easily observed in the periodic optics of the bypass line in Figure 11, where the vertical scale is chosen to emphasize the beam size in the bypass area. At σ_δ = 0.1% the maximum rms beam size of $\sigma \approx 0.1$ mm in the bypass is nearly the nominal value, while at σ_δ = 1.2% it grows by more than ten-fold to $\sigma \approx 1.7$ mm. This large beam size not only degrades the beam quality for FEL but also results in particle loss on collimators. With the missing bypass dogleg sextupoles, the losses occur at $\sigma_\delta > 0.7\%$ as follows from Figure 9.

Based on the above evaluation, one can conclude that at small $\sigma_\delta \leq 0.2\%$ the second order dispersion correction is not critical, and the sextupoles may not be necessary under these conditions. At large σ_δ the emittance growth without the sextupoles can quickly become very large, hence there is the need of the sextupole correction to compensate this effect.

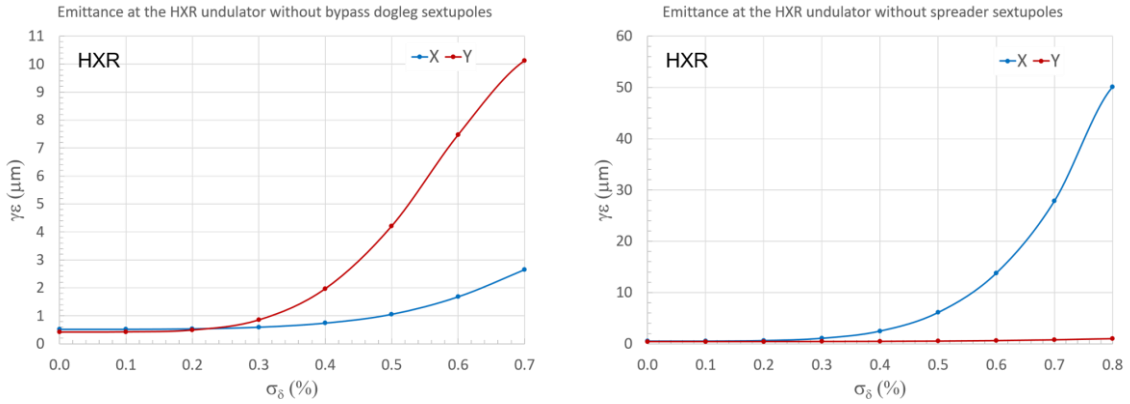

Figure 9: HXR emittance vs σ_δ where sextupoles are turned off in the bypass dogleg (left) or HXR spreader (right). The plotted range corresponds to maximum σ_δ where there is no beam loss on the collimators.

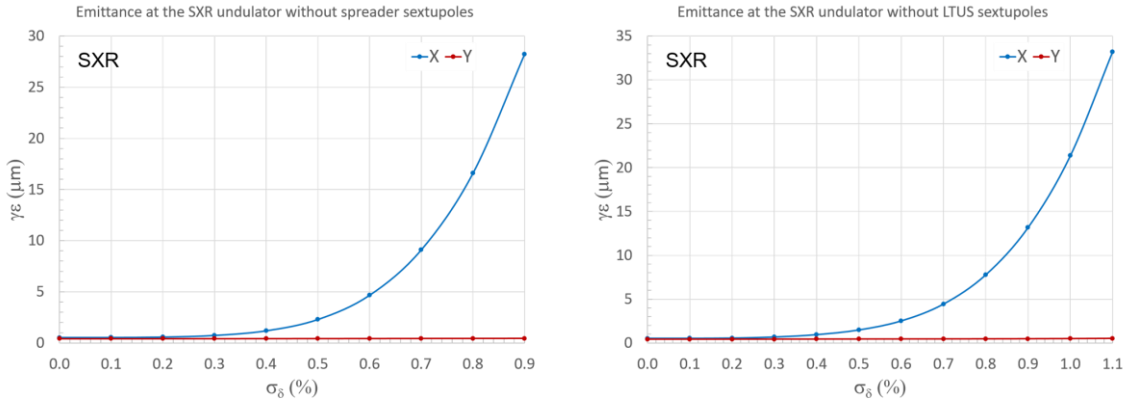

Figure 10: SXR emittance vs σ_δ where sextupoles are turned off in the SXR spreader (left) or SXR LTU dogleg (right). The plotted range corresponds to maximum σ_δ where there is no beam loss on the collimators.

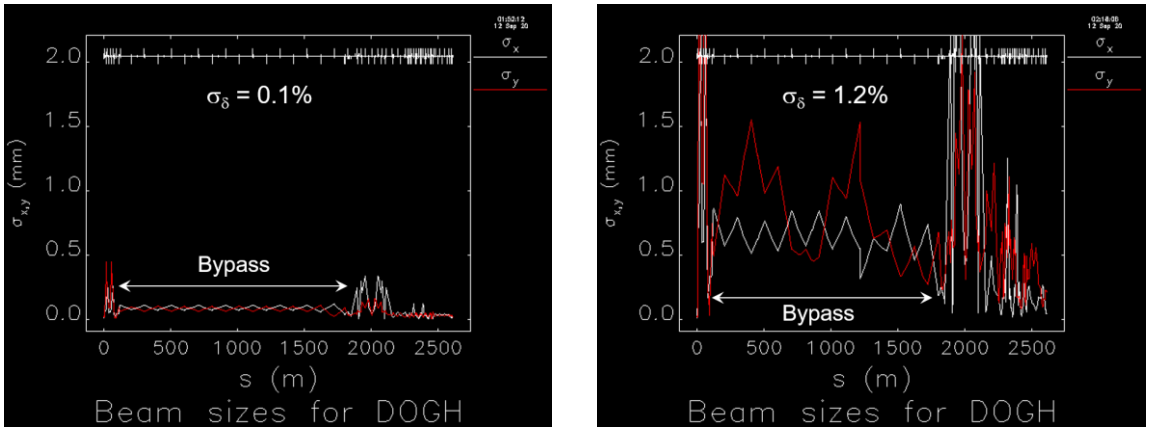

Figure 11: HXR rms beam size in the LCLS-II-HE at σ_δ = 0.1% (left) and 1.2% (right) with bypass dogleg sextupoles turned off.

3 Sextupole misalignment

Analysis of emittance growth in the previous section established the benefit of the second order dispersion correction in the LCLS-II-HE; it reduces the emittance at large σ_δ by more than a factor of 10. The above

calculations, however, were performed under ideal conditions without magnet errors. Unavoidable sextupole alignment errors create another source of emittance growth; the latter would negate some of the emittance reduction due to the sextupole correction. Therefore, it is important to evaluate the emittance growth including the effect of sextupole *x* and *y* offset errors in order to determine if the sextupole correction under these conditions is still beneficial for the emittance control. This analysis will also allow us to estimate the sextupole alignment tolerances.

3.1 Analytic emittance estimate

Analytic emittance growth due to sextupole horizontal and vertical misalignment is derived in [1] in the limit of normal sextupoles (no roll) and horizontal dispersion. Since some of the LCLS-II-HE sextupoles are rolled with respect to the normal position and located where there is both horizontal and vertical dispersion, we expand the derivation to include these conditions using the same method as in [1] – see Appendix for details. The resulting expressions for the emittance growth as a function of sextupole X and Y error offsets are:

$$\frac{\Delta\varepsilon_x}{\varepsilon_{x0}} = \frac{\beta_x}{2\varepsilon_{x0}}(K_2L)^2\{X^2[C_3^2\sigma_{x0}^2 + S_3^2\sigma_{y0}^2 + S_6\eta_x\eta_y\sigma_\delta^2] + Y^2[S_3^2\sigma_{x0}^2 + C_3^2\sigma_{y0}^2 - S_6\eta_x\eta_y\sigma_\delta^2] + XY[S_6(\sigma_{x0}^2 - \sigma_{y0}^2) - 2C_6\eta_x\eta_y\sigma_\delta^2]\} \quad (2)$$

$$\frac{\Delta\varepsilon_y}{\varepsilon_{y0}} = \frac{\beta_y}{2\varepsilon_{y0}}(K_2L)^2\{X^2[S_3^2\sigma_{x0}^2 + C_3^2\sigma_{y0}^2 - S_6\eta_x\eta_y\sigma_\delta^2] + Y^2[C_3^2\sigma_{x0}^2 + S_3^2\sigma_{y0}^2 + S_6\eta_x\eta_y\sigma_\delta^2] - XY[S_6(\sigma_{x0}^2 - \sigma_{y0}^2) - 2C_6\eta_x\eta_y\sigma_\delta^2]\} \quad (3)$$

$$\sigma_{x0}^2 = \beta_x\varepsilon_{x0} + \eta_x^2\sigma_\delta^2\,; \quad \sigma_{y0}^2 = \beta_y\varepsilon_{y0} + \eta_y^2\sigma_\delta^2 \quad (4)$$

$$S_3 = \sin(3\psi)\,; \quad C_3 = \cos(3\psi)\,; \quad S_6 = \sin(6\psi)\,; \quad C_6 = \cos(6\psi) \quad (5)$$

Here, K_2 and L are the sextupole K-value and the effective length, respectively; X,Y (capital) are the sextupole horizontal and vertical error offsets; $\gamma\varepsilon_{x0}$ = 0.52 μm-rad, $\gamma\varepsilon_{y0}$ = 0.42 μm-rad are the initial *x* and *y* normalized emittances; σ_δ is the rms relative energy spread; β_x, β_y and η_x, η_y are beta functions and linear dispersion at the sextupole, respectively; and ψ is the sextupole roll angle (positive angle corresponds to clockwise rotation when looking at the sextupole from upstream).

The emittance growth is quadratic with the X, Y misalignment, the sextupole strength, and the rms energy spread. At large enough σ_δ, the non-linear dispersion may need to be taken into account. For the case of normal sextupoles and only horizontal dispersion such as in the SXR spreader and the SXR LTU dogleg the Eqs. (2) and (3) are reduced to the same result as in [1]:

$$\frac{\Delta\varepsilon_x}{\varepsilon_{x0}} = \frac{\beta_x}{2\varepsilon_{x0}}(K_2L)^2\{X^2\sigma_{x0}^2 + Y^2\sigma_{y0}^2\} = \frac{1}{2}\beta_x^2(K_2L)^2\left\{X^2\left(1 + \frac{\eta_x^2\sigma_\delta^2}{\beta_x\varepsilon_{x0}}\right) + Y^2\frac{\beta_y\varepsilon_{y0}}{\beta_x\varepsilon_{x0}}\right\} \quad (6)$$

$$\frac{\Delta\varepsilon_y}{\varepsilon_{y0}} = \frac{\beta_y}{2\varepsilon_{y0}}(K_2L)^2\{X^2\sigma_{y0}^2 + Y^2\sigma_{x0}^2\} = \frac{1}{2}\beta_x\beta_y\left(\frac{\varepsilon_{x0}}{\varepsilon_{y0}}\right)(K_2L)^2\left\{X^2\frac{\beta_y\varepsilon_{y0}}{\beta_x\varepsilon_{x0}} + Y^2\left(1 + \frac{\eta_x^2\sigma_\delta^2}{\beta_x\varepsilon_{x0}}\right)\right\} \quad (7)$$

The LCLS-II-HE sextupole parameters, to be used in Eqs. (2) – (7), are listed in Table 1. Based on these parameters, one can see that for the normal sextupoles SSP1S, SSP2S, SDL1, SDL2 the factor $\frac{\eta_x^2\sigma_\delta^2}{\beta_x\varepsilon_{x0}}$ is dominant in Eqs. (6), (7) at the typical and large σ_δ, hence these sextupoles are expected to create mostly horizontal emittance growth with the X-offset and vertical emittance growth with the Y-offset. The four rolled sextupoles in the bypass dogleg and the HXR spreader, where dispersion is in both planes, create both *x* and *y* emittance growth with either X or Y offsets.

Table 1: LCLS-II-HE sextupole parameters per LCLS-II-HE lattice version of July 04, 2020.

Name	K_2, m^{-3}	L, m	ψ, rad	β_x, m	β_y, m	η_x, m	η_y, m
SDOG1	-9.189	0.1	-0.23130	5.954	31.249	0.09069	-0.44059
SDOG2	22.656	0.1	0.29200	31.242	5.955	-0.25146	0.17378
SSP1H	-20.985	0.1	0.26609	99.413	81.125	-0.23543	2.2E-05
SSP2H	22.591	0.1	0.31073	65.647	49.562	0.28983	0.05085
SSP1S	12.699	0.1	0	77.803	75.272	0.34262	0
SSP2S	12.697	0.1	0	77.817	75.240	0.34265	0
SDL1	-8.735	0.1	0	42.390	7.680	-0.43215	0
SDL2	-24.395	0.1	0	42.386	7.679	-0.15472	0

3.2 Sextupole misalignment and small energy spread

Tracking simulations are performed using `elegant` to determine the emittance growth versus *x* and *y* offset errors of individual sextupoles. This also allows us to estimate the sextupole alignment tolerances. Results of the simulations in this section are for a small $\sigma_\delta = 0.1\%$; they are compared with the analytic estimates from Eqs. (2) and (3). The `elegant` tracking setup and the initial beam are described in Section 2.2. In the simulations, all the sextupoles are turned on, and either a horizontal or vertical offset error is assigned to one selected sextupole while all other magnets have no errors. The emittance is determined at entrance of the HXR and SXR undulators for a range of sextupole offset errors.

Emittance growth versus X and Y sextupole offsets is presented in Figure 12 to Figure 15, where both the `elegant` and analytic results are plotted. Note that the simulation results include contributions to the emittance from both the misalignment and the higher order dispersion (although the latter is very small at the small σ_δ), while the analytic estimates take into account only the effect of misalignment. The range of σ_δ in these plots is intentionally limited to 0.02; this allows for a direct estimate of sextupole alignment tolerances corresponding to 2% of emittance growth. The `elegant` and analytic results at this small σ_δ agree very well. The emittance growth exhibits a nearly symmetric quadratic dependence on X and Y offsets as predicted in Eqs. (2) and (3), therefore it is sufficient to plot only the positive X and Y range. Based on these results, the estimated sextupole alignment tolerances at $\sigma_\delta = 0.1\%$ are roughly ≥ 300 μm which are relatively loose.

In summary, for typical LCLS-II-HE beam conditions with ~0.1% rms energy spread the sextupole correction of the second order dispersion is not critical. If the sextupoles are included, it should be straightforward to satisfy the relatively loose sextupole alignment tolerances.

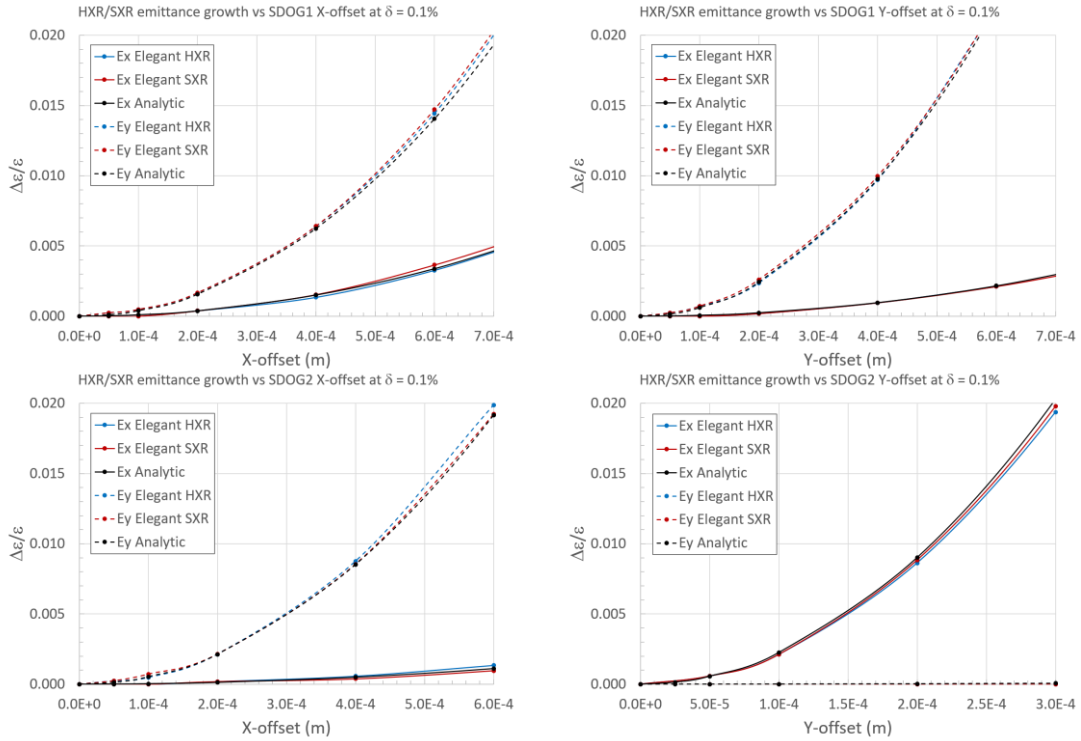

Figure 12: HXR and SXR emittance growth vs X (left) and Y (right) offsets of the bypass dogleg sextupoles SDOG1 (top) and SDOG2 (bottom) at σ_δ = 0.1%. The results are from `elegant` simulations and analytic estimates.

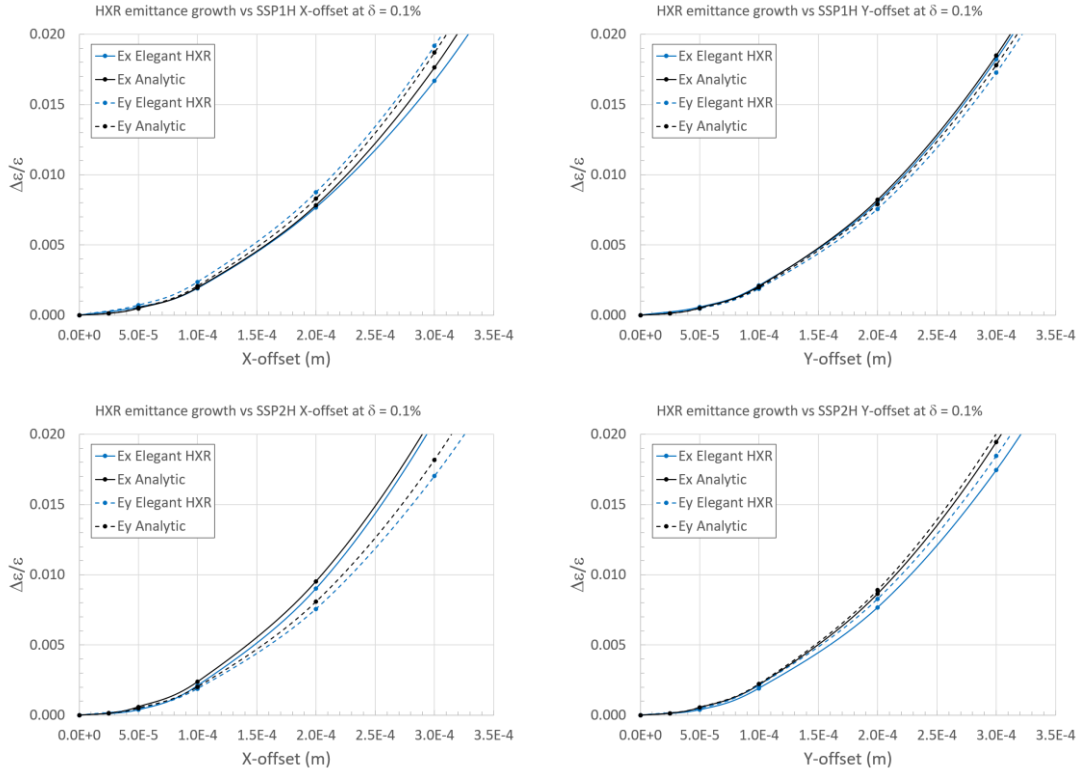

Figure 13: HXR emittance growth vs X (left) and Y (right) offsets of the HXR spreader sextupoles SSP1H (top) and SSP2H (bottom) at σ_δ = 0.1%. The results are from `elegant` simulations and analytic estimates.

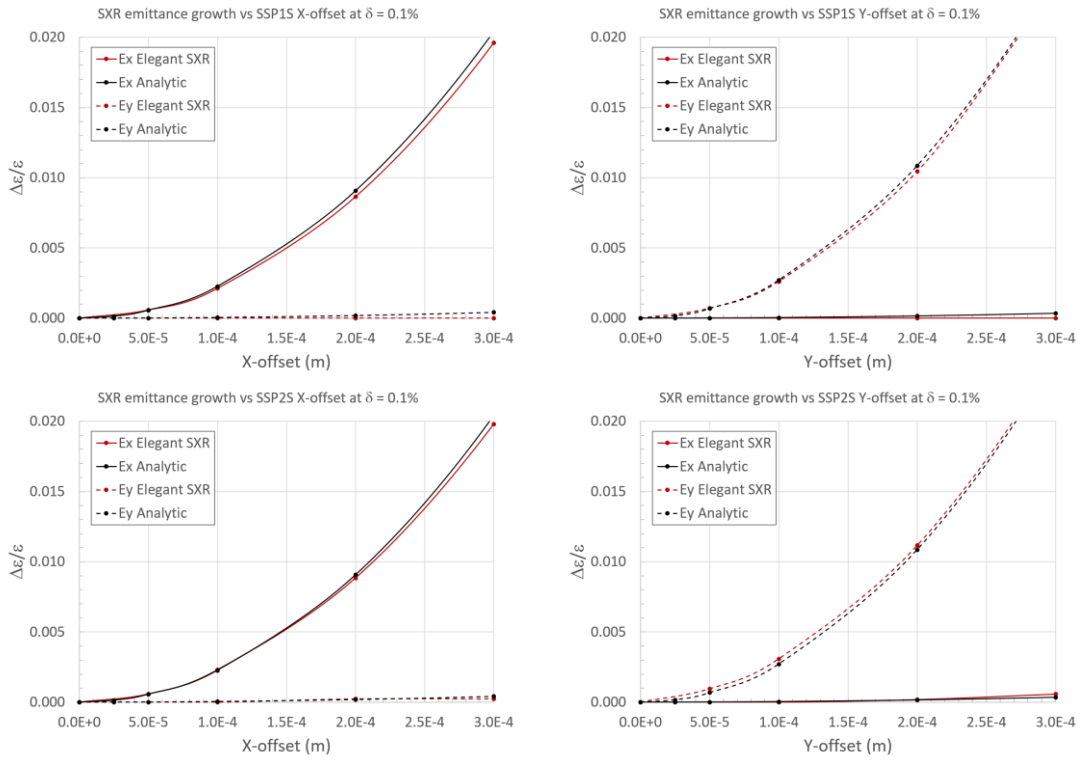

Figure 14: SXR emittance growth vs X (left) and Y (right) offsets of the SXR spreader sextupoles SSP1S (top) and SSP2S (bottom) at σ_δ = 0.1%. The results are from `elegant` simulations and analytic estimates.

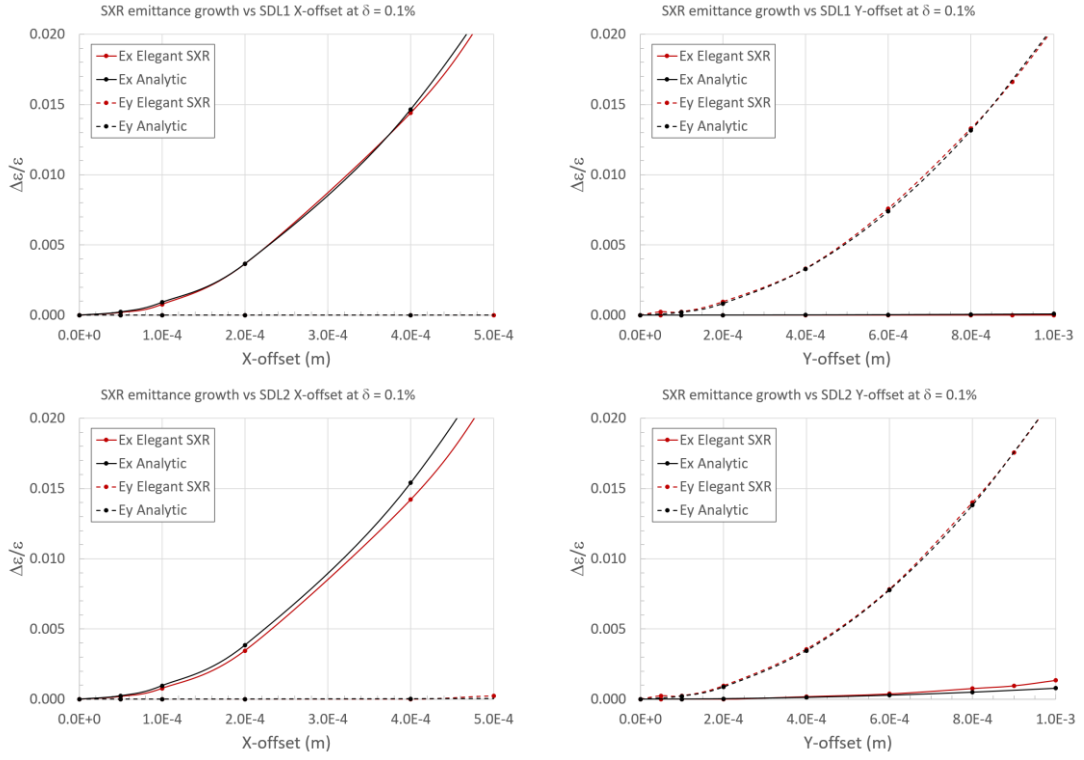

Figure 15: SXR emittance growth vs X (left) and Y (right) offsets of the SXR LTU dogleg sextupoles SDL1 (top) and SDL2 (bottom) at σ_δ = 0.1%. The results are from `elegant` simulations and analytic estimates.

3.3 Sextupole misalignment and large energy spread

In this section, the emittance growth versus sextupole *x* and *y* misalignment is evaluated for a large energy spread with σ_δ = 0.5%. Results from `elegant` tracking are presented in Figure 16 to Figure 19, where each plot corresponds to one misaligned sextupole while the other magnets are error free. As in the previous section, the plotted range of emittance growth is 0.02, suitable for direct estimate of alignment tolerances. The tracking includes the effects from both the sextupole misalignment and the non-linear dispersion. The latter cannot be ignored at the large energy spread; for this reason we do not compare these simulations with the analytic estimates of Eqs. (2), (3) which take into account only the misalignment in the limit of first order dispersion. Since the LCLS-II-HE beamline splits into separate HXR and SXR lines with different optics, the non-linear dispersion and its impact on emittance are somewhat different in the HXR and SXR even for the shared sextupoles in the bypass dogleg. The emittance values are determined at entrance of the HXR and SXR undulators for a range of sextupole offset errors.

As in the case of σ_δ = 0.1%, emittance growth at σ_δ = 0.5% depends quadratically on X and Y offsets, but exhibits asymmetry with X and Y. For this reason, some of the plots in Figure 16 to Figure 19 are expanded to include negative X and Y values in order to determine the tolerances. The consequence of the asymmetry is that the emittance is minimized at a non-zero sextupole offset, although the typical emittance reduction is small – on the order of 1%. Trying to understand this result, we inspect the electron distribution at a misaligned sextupole. Since the effect becomes evident at a large energy spread, it should be related to non-linear dispersion which increases more rapidly at large δ than the linear term. To lowest order, we examine the effect of electron position displacement $\Delta x = \eta_1 \delta + \eta_2 \delta^2$ at a sextupole due to the first and second order dispersion (η_1 and η_2), assuming symmetric energy spread and symmetric initial *x*-*y* betatron distribution as used in the study.

First, it should be noted that the electron's displacements due to the first order dispersion ($\eta_1\delta$) are symmetric relative to beam center, thus preserving the beam size symmetry. However, displacements due to the second order dispersion ($\eta_2\delta^2$) are of the same sign for positive and negative δ, thus creating the asymmetry. In this case, electrons on one side of the beam distribution have larger amplitudes than on the other side. This leads to asymmetry of the sextupole field seen by electrons on the positive and negative sides of the beam. For small σ_δ, this asymmetry is small, therefore emittance growth is about the same for positive and negative sextupole offsets. For larger σ_δ, the beam distribution becomes more asymmetric, therefore the emittance growth may depend on the direction in which the sextupole is offset relative to the beam. Based on the results, there is an "optimal" sextupole offset which minimizes the emittance, possibly by moving the sextupole in a position where beam distribution is better symmetrized relative to the sextupole center, so the net effect of the sextupole kick is minimized. This result suggests that if one can make the sextupole offset adjustable and controllable with enough accuracy, it could be used as a fine tuning emittance knob.

In cases of the rolled sextupoles where dispersion is in *x* and *y* planes, the emittance growth is asymmetric relative to both X and Y offsets – see Figure 16 and Figure 17. For normal sextupoles and only the horizontal dispersion, the asymmetry is primarily caused by the X-offsets as can be seen in Figure 18 and Figure 19.

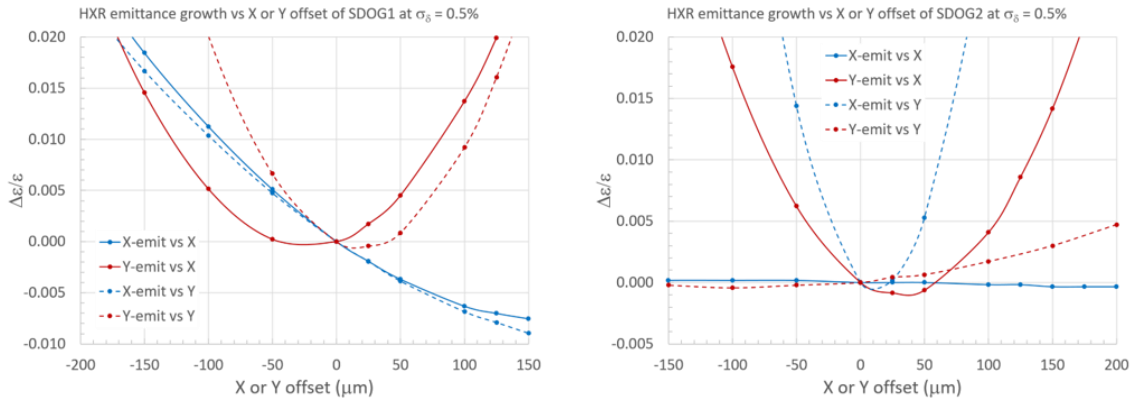

Figure 16: HXR emittance growth vs X and Y-offsets of the bypass dogleg sextupoles SDOG1 (left) and SDOG2 (right) at σ_δ = 0.5%. The results are from `elegant` simulations.

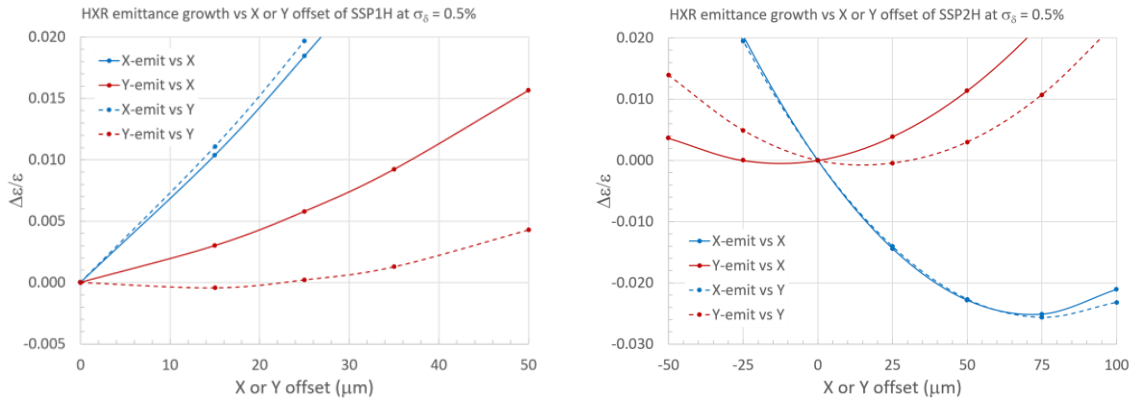

Figure 17: HXR emittance growth vs X and Y-offsets of the HXR spreader sextupoles SSP1H (left) and SSP2H (right) at σ_δ = 0.5%. The results are from `elegant` simulations.

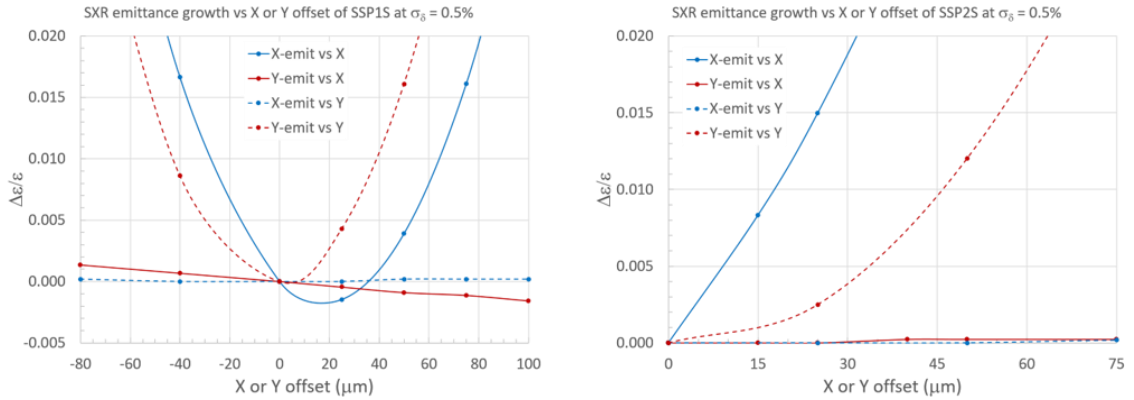

Figure 18: SXR emittance growth vs X and Y-offsets of the SXR spreader sextupoles SSP1S (left) and SSP2S (right) at σ_δ = 0.5%. The results are from `elegant` simulations.

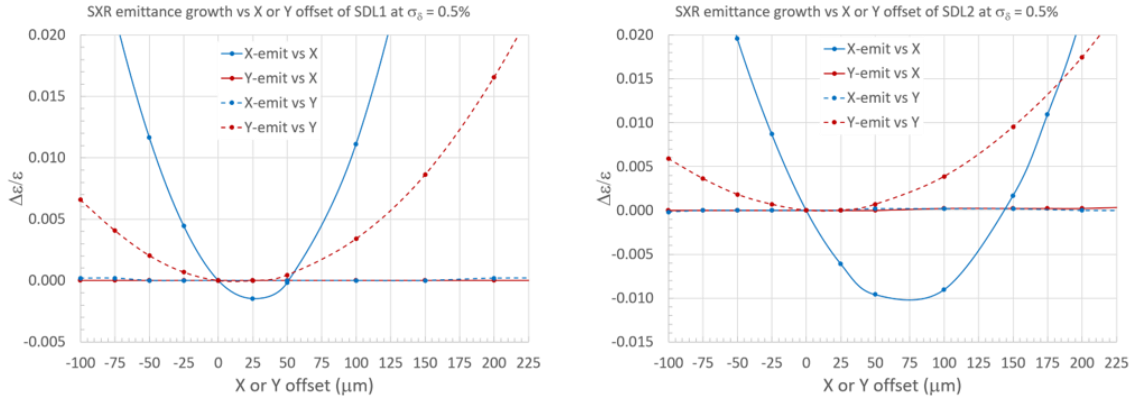

Figure 19: SXR emittance growth vs X and Y-offsets of the SXR LTU dogleg sextupoles SDL1 (left) and SDL2 (right) at σ_δ = 0.5%. The results are from `elegant` simulations.

Sextupole alignment tolerances, X_{tol} and Y_{tol}, at σ_δ = 0.5% are estimated from the results in Figure 16 to Figure 19, corresponding to 2% emittance growth from a single sextupole. These tolerances are in the range from 25 μm to about 200 μm which are significantly tighter than at σ_δ = 0.1%. The estimated tolerances for both σ_δ = 0.1% and 0.5% are listed in Table 2. The tolerance scaling with the energy spread can be roughly determined from the Eqs. (2), (3) and (6), (7) assuming dispersion dominated beam size and the limit of the

first order dispersion. In this approximation, the x and y tolerances are inversely proportional to σ_δ. Consequently, the tolerances at $\sigma_\delta = 0.5\%$ should be a factor of five tighter than at $\sigma_\delta = 0.1\%$. Based on the `elegant` tracking and Table 2 results, the actual ratio of the tolerances in these two cases is in the range of $\approx 4 - 12$ for the different sextupoles and two planes. The most challenging tolerances are for the spreader sextupoles at $\sigma_\delta = 0.5\%$, particularly in the HXR spreader. Tolerances for the shared bypass dogleg sextupoles SDOG1, SDOG2 are based on the HXR values since the corresponding SXR tolerances are slightly looser.

Table 2: Sextupole alignment tolerances X_{tol}, Y_{tol} corresponding to 2% emittance growth (ε_x or ε_y – whichever is larger) from x or y misalignment of a single sextupole for $\sigma_\delta = 0.1\%$ and 0.5% (flat energy spread) based on `elegant` tracking.

Name	$\sigma_\delta = 0.1\%$		$\sigma_\delta = 0.5\%$	
	X_{tol}, μm	Y_{tol}, μm	X_{tol}, μm	Y_{tol}, μm
SDOG1	700	560	125	100
SDOG2	600	300	110	65
SSP1H	305	310	27	25
SSP2H	290	310	25	25
SSP1S	300	270	45	55
SSP2S	300	270	32	65
SDL1	460	1000	70	220
SDL2	460	950	50	220

3.4 Realistic sextupole misalignment

Results of the previous sections established that an uncompensated second order dispersion in combination with a large energy spread generates an excessive emittance growth in the LCLS-II-HE. Local cancellation of the second order dispersion using sextupoles significantly reduces this effect. However, at large energy spread the sextupoles require tight alignment tolerances to limit the emittance growth due to sextupole misalignment. Based on Table 2, at $\sigma_\delta = 0.5\%$ tolerances for some of the sextupoles are as tight as ~25 μm which are challenging. These tolerances, however, are defined for 2% of emittance growth due to a single sextupole offset. This 2% emittance growth is very small compared to the emittance growth without sextupoles ($\frac{\varepsilon}{\varepsilon_0} \sim 10$ at $\sigma_\delta = 0.5\%$), even if the effects of all sextupoles with the tolerance errors are combined. For this reason it is reasonable to consider somewhat looser, but more realistic alignment errors and verify if the sextupole correction still provides significant emittance reduction. To investigate this scenario, we perform `elegant` tracking at $\sigma_\delta = 0.5\%$, where randomly generated X and Y sextupole offsets with realistically achievable rms of $\sigma_{x,y} = 100$ μm are used.

As in the previous simulations, the beam is tracked from the beginning of the bypass dogleg to the entrance of the HXR and SXR undulators, where the initial beam is described in Section 2.2 and the energy spread is flat with $\sigma_\delta = 0.5\%$. All the sextupoles are turned on to correct the second order dispersion. The effect of sextupole misalignment is evaluated separately for each bending section where the sextupole offsets are applied, while there are no errors in other sections. The sextupole offsets are randomly generated with the Gaussian rms of $\sigma_{x,y} = 100$ μm. For each case, the tracking is done for 10 different sets (seeds) of random errors in order to evaluate the range of emittance variation. Results of the simulations are presented in Figure 20 to Figure 24, where each Figure corresponds to misaligned sextupoles in one section, and the two plots show the normalized emittance ($\gamma\varepsilon$) and the relative emittance growth ($\Delta\varepsilon/\varepsilon_0$) for each seed. Emittance without misalignment is also shown which is used as a reference value for emittance growth calculation. Finally, emittance where the respective sextupoles are turned off is also plotted. Comparison of the emittance

growth in two cases: 1) with the sextupole correction and misalignment, and 2) without sextupoles, allows one to decide if the sextupole correction in the LCLS-II-HE is beneficial for emittance reduction.

All the sextupole random offsets used in the simulations are listed in Table 3. The average and rms values of normalized emittance and emittance growth in 10 seeds are presented in Table 4. Emittance where the corresponding sextupoles are turned off is also included in Table 4. The results are consistent with the alignment tolerances in Table 2. For example, the largest emittance growth is generated by the SSP1H and SSP2H sextupoles which have the tightest tolerances in Table 2. As can be seen in Table 4, the emittance growth ($\Delta\varepsilon/\varepsilon_0$) with the 100 μm rms sextupole misalignment is in the range of a few % to tens of %, and the resulting emittance ($\gamma\varepsilon$) is much smaller than the emittance without the sextupoles by a factor of a few to 10.

These results justify the use of the sextupole correction in the LCLS-II-HE which yields much smaller beam emittance in scenarios with large energy spread as compared to emittance without sextupoles, taking into account realistically achievable sextupole alignment errors of the order of 100 μm (rms).

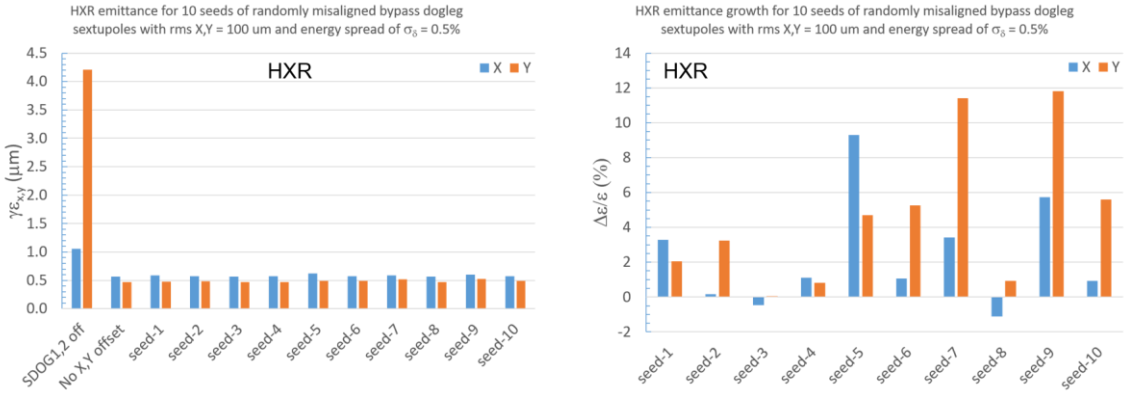

Figure 20: HXR normalized emittance (left) and emittance growth (right) at σ_δ = 0.5% for 10 seeds of randomly misaligned bypass dogleg sextupoles SDOG1 and SDOG2 with rms X,Y offsets of 100 microns. The left figure also shows emittance without misalignment and with the SDOG1, SDOG2 turned off. Other sextupoles are on.

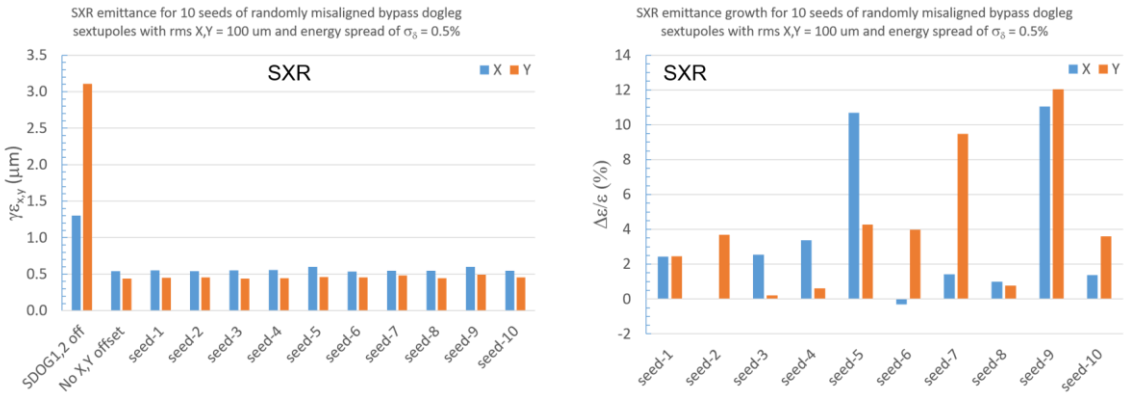

Figure 21: SXR emittance (left) and emittance growth (right) at σ_δ = 0.5% for 10 seeds of randomly misaligned bypass dogleg sextupoles SDOG1 and SDOG2 with rms X,Y offsets of 100 microns. The left figure also shows emittance without misalignment and with the SDOG1, SDOG2 turned off. Other sextupoles are on.

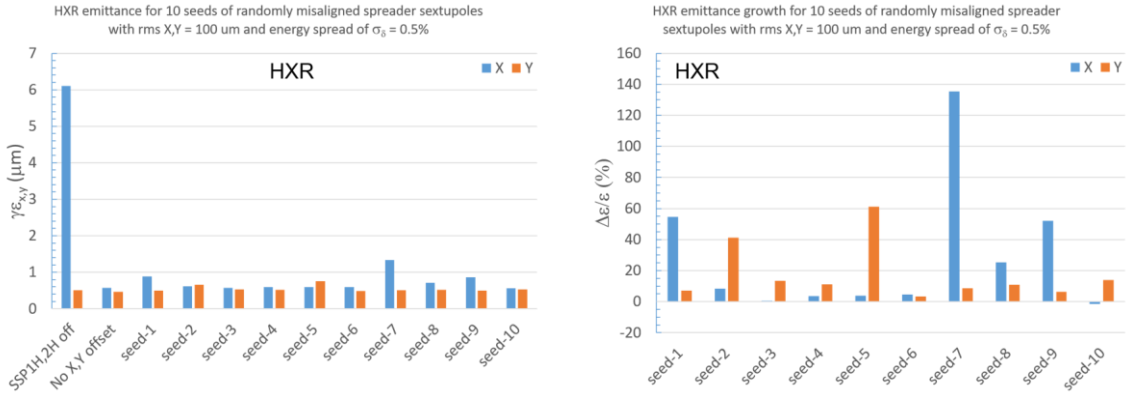

Figure 22: HXR emittance (left) and emittance growth (right) at σ_δ = 0.5% for 10 seeds of randomly misaligned HXR spreader sextupoles SSP1H and SSP2H with rms X,Y offsets of 100 microns. The left figure also shows emittance without misalignment and with the SSP1H, SSP2H turned off. Other sextupoles are on.

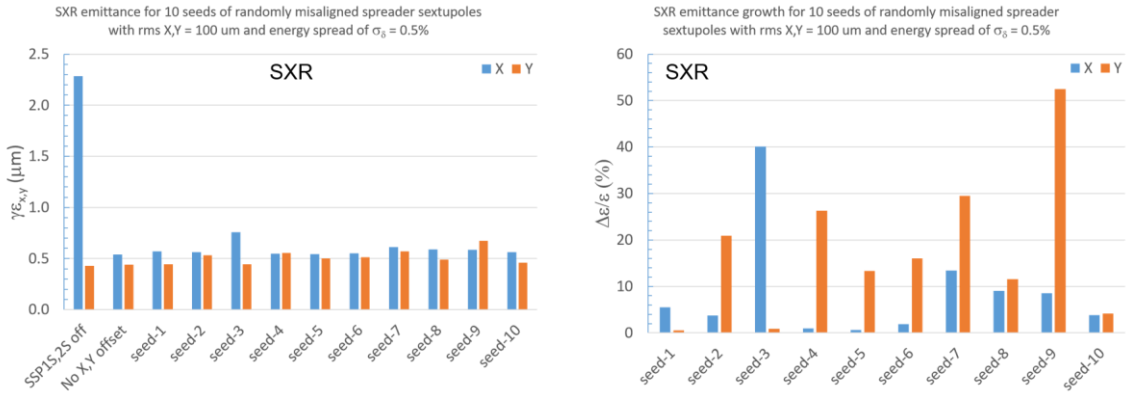

Figure 23: SXR emittance (left) and emittance growth (right) at σ_δ = 0.5% for 10 seeds of randomly misaligned SXR spreader sextupoles SSP1S and SSP2S with rms X,Y offsets of 100 microns. The left figure also shows emittance without misalignment and with the SSP1S, SSP2S turned off. Other sextupoles are on.

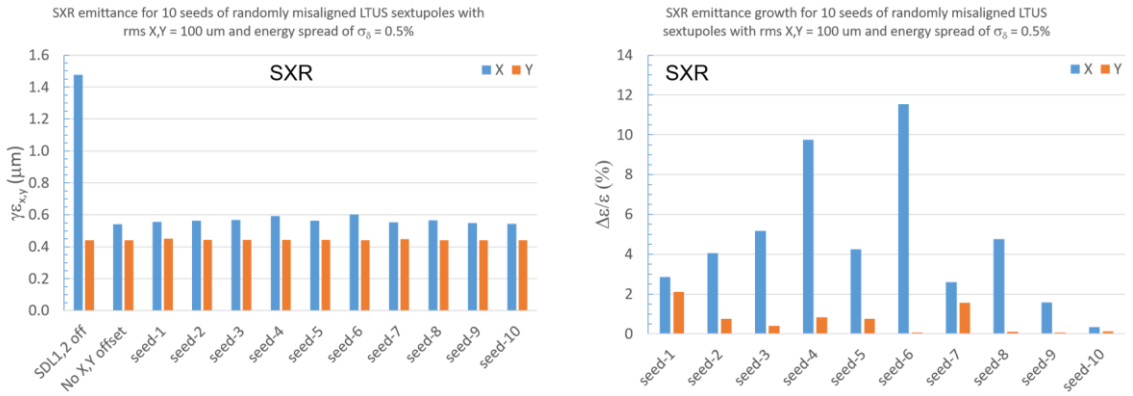

Figure 24: SXR emittance (left) and emittance growth (right) at σ_δ = 0.5% for 10 seeds of randomly misaligned SXR LTU dogleg sextupoles SDL1 and SDL2 with rms X,Y offsets of 100 microns. The left figure also shows emittance without misalignment and with the SDL1, SDL2 turned off. Other sextupoles are on.

Table 3: Random X and Y sextupole offsets (μm) in seeds 1–10.

Name	Plane	Random seeds									
		1	2	3	4	5	6	7	8	9	10
SDOG1	X	-148.3	-108.9	55.1	-18.7	-7.2	36.8	69.8	12.8	-27.7	18.7
	Y	43.5	102.4	68.7	76.7	-1.5	-123.0	-202.9	111.3	304.6	-22.6
SDOG2	X	-30.9	-28.4	34.5	-121.0	212.5	-26.6	-13.8	-145.8	-44.7	-163.4
	Y	64.9	17.0	67.4	93.4	-161.7	-17.2	-70.0	22.3	-94.5	-29.0
SSP1H	X	125.5	-112.1	-129.4	-108.5	198.3	34.0	199.9	51.1	13.5	-113.6
	Y	58.7	-216.5	71.6	-81.8	-100.6	-69.6	175.7	67.7	-38.8	48.7
SSP2H	X	-36.0	24.5	40.9	97.7	95.0	-53.0	-34.0	-121.7	-132.2	-2.1
	Y	-92.3	-242.1	67.8	-112.3	-49.5	-31.5	-145.9	59.9	-192.2	69.9
SSP1S	X	-102.0	-118.7	-113.2	46.2	37.2	36.8	-63.1	66.0	-62.6	89.4
	Y	-29.1	196.0	-32.8	-164.8	155.9	-175.5	-191.4	-88.2	-265.6	-57.9
SSP2S	X	-21.2	-154.7	188.4	21.0	16.0	40.5	83.9	119.4	56.4	-49.1
	Y	22.6	-43.5	31.6	215.8	-60.4	27.2	-85.1	-91.2	-111.9	-49.9
SDL1	X	41.9	-89.2	107.1	-100.0	140.1	-34.7	50.9	179.3	-83.1	12.0
	Y	82.5	-62.6	-80.2	-116.8	12.8	36.3	15.9	5.2	-20.9	-42.1
SDL2	X	-66.9	-35.3	-83.1	-124.2	-36.9	-176.6	-60.9	14.4	67.0	-13.8
	Y	190.8	122.0	21.4	68.6	134.0	45.4	188.3	58.6	10.6	17.9

Table 4: Average and rms values of emittance and emittance growth in `elegant` tracking at σ_δ = 0.5% for 10 seeds of random alignment errors applied to sextupoles of a given section. For comparison, emittance with the corresponding sextupoles turned off is also shown.

	Sextupoles off		10 random seeds							
	γε, μm		<γε>, μm		rms γε, μm		<Δε/ε>, %		rms Δε/ε, %	
NAME	X	Y	X	Y	X	Y	X	Y	X	Y
SDOG1, SDOG2 (HXR)	1.056	4.207	0.583	0.488	0.017	0.018	2.3	4.6	3.0	4.0
SDOG1, SDOG2 (SXR)	1.303	3.105	0.559	0.459	0.021	0.016	3.4	4.1	3.9	3.7
SSP1H, SSP2H	6.104	0.511	0.733	0.549	0.231	0.082	28.7	17.7	40.7	17.6
SSP1S, SSP2S	2.284	0.430	0.588	0.518	0.060	0.066	8.8	17.6	11.1	15.0
SDL1, SDL2	1.477	0.441	0.566	0.444	0.018	0.003	4.7	0.7	3.3	0.7

4 Conclusions

The study showed that uncompensated second order dispersion in the LCLS-II-HE creates an excessive emittance growth in beam conditions with large energy spread. Eight sextupoles included in the bypass dogleg, HXR and SXR spreader lines, and SXR LTU dogleg provide an effective local correction of the second order dispersion. Although this correction is not critical at small energy spread ($\sigma_\delta \leq 0.2\%$) where the effect of the second order dispersion is small, it is essential for reducing a very large emittance growth at a larger energy spread. The effectiveness of the correction is somewhat decreased by emittance growth caused by sextupole misalignment; however, the tracking study with large energy spread ($\sigma_\delta = 0.5\%$) and reasonable rms alignment errors (100 μm) demonstrated that the emittance reduction due to the sextupole correction is by far more significant than emittance growth due to misalignment. It is, therefore, concluded that the sextupole system in the LCLS-II-HE is justified by significant reduction of the beam emittance in scenarios with large energy spread.

5 Appendix

Emittance growth due to sextupole misalignment is derived analytically in [1] in the assumption of normal sextupoles (no roll angle) and horizontal dispersion. Here, we use the same method to expand the derivation to the case where sextupoles are rolled with respect to the normal position and have both horizontal and vertical dispersion.

We start with the general equation of relative emittance growth due to perturbation of angular coordinates $\Delta x'$, $\Delta y'$ derived in [1]:

$$\frac{\Delta\varepsilon_x}{\varepsilon_{x0}} = \frac{\beta_x}{2\varepsilon_{x0}}\langle\Delta x'^2\rangle, \qquad \frac{\Delta\varepsilon_y}{\varepsilon_{y0}} = \frac{\beta_y}{2\varepsilon_{y0}}\langle\Delta y'^2\rangle \tag{8}$$

In case of sextupole *x* and *y* misalignment, the $\Delta x'$, $\Delta y'$ represent the change of the electron horizontal and vertical angular coordinates at the sextupole due to the misalignment; ε_{x0}, ε_{y0} are the unperturbed horizontal and vertical un-normalized emittances; β_x, β_y are beta functions at the sextupole, and the brackets < > represent an average over the electron distribution. Similar to [1], to simplify the analysis, we treat the sextupole effect due to misalignment in thin-lens approximation.

To solve the Eq. (8), we need to derive the expressions for $\Delta x'$, $\Delta y'$ caused by the sextupole offsets. The angular kick is the result of the change of the field seen by the electrons in misaligned sextupole as compared to the ideal sextupole field. We will denote this change of the field by ΔB_x and ΔB_y. In general, the change of particle angular coordinates $\Delta x'$, $\Delta y'$ due to magnetic field error is

$$\Delta x' = -\frac{\Delta B_y L}{B\rho}, \qquad \Delta y' = \frac{\Delta B_x L}{B\rho} \tag{9}$$

where L is the magnet effective length, and Bρ is magnetic rigidity.

The B_x and B_y field components of a rolled sextupole in *x-y* coordinate system centered at the ideal sextupole center can be written as

$$B_y = \frac{B''}{2} C_3 (x^2 - y^2) + B'' S_3 xy \tag{10}$$

$$B_x = B'' C_3 xy - \frac{B''}{2} S_3 (x^2 - y^2) \tag{11}$$

where $B'' = K_2 B\rho$ is the second order derivative of the field, $C_3 = \cos(3\psi)$, $S_3 = \sin(3\psi)$, and ψ is the roll angle. To determine the change of the sextupole field ΔB seen by electrons due to the misalignment, we express the electron coordinates at the sextupole as

$$x = x_\beta + \eta_x \delta - X \tag{12}$$

$$y = y_\beta + \eta_y \delta - Y \tag{13}$$

where x_β, y_β are unperturbed betatron coordinates in absence of dispersion, η_x, η_y are the horizontal and vertical linear dispersion functions, δ is the electron relative momentum error, and X, Y are the horizontal and vertical sextupole offsets due to the misalignment.

We then insert the *x* and *y* expressions from Eqs. (12) and (13) into Eqs. (10) and (11), and find the ΔB_y and ΔB_x due to misalignment by keeping only the field terms proportional to X and Y. Note that the field terms proportional to X^2, Y^2 and XY are not relevant here since they cause simple orbit steering which will be compensated. The resulting ΔB_y and ΔB_x are then substituted into Eq. (9), yielding:

$$\Delta x' = K_2 L\{X[C_3(x_\beta + \eta_x\delta) + S_3(y_\beta + \eta_y\delta)] + Y[S_3(x_\beta + \eta_x\delta) - C_3(y_\beta + \eta_y\delta)]\} \tag{14}$$

$$\Delta y' = K_2 L\{X[S_3(x_\beta + \eta_x\delta) - C_3(y_\beta + \eta_y\delta)] - Y[C_3(x_\beta + \eta_x\delta) + S_3(y_\beta + \eta_y\delta)]\} \tag{15}$$

The resulting angular kick is proportional to X and Y sextupole offsets. Next, using the expressions in Eqs. (14), (15), we find the averages $<\Delta x'^2>$ and $<\Delta y'^2>$ over electron distribution, where x_β, y_β and δ are randomly distributed and independent of each other with zero mean values. In this case, only the terms proportional to $\langle x_\beta^2\rangle = \beta_x \varepsilon_{x0}$, $\langle y_\beta^2\rangle = \beta_y \varepsilon_{y0}$, and $\langle \delta^2\rangle = \sigma_\delta^2$ remain, while $\langle x_\beta \delta\rangle = \langle y_\beta \delta\rangle = 0$. Substituting the resulting $<\Delta x'^2>$ and $<\Delta y'^2>$ into Eq. (8) yields the final expressions for the emittance growth as a function of sextupole X and Y offsets:

$$\frac{\Delta\varepsilon_x}{\varepsilon_{x0}} = \frac{\beta_x}{2\varepsilon_{x0}} (K_2 L)^2 \{X^2[C_3^2\sigma_{x0}^2 + S_3^2\sigma_{y0}^2 + S_6\eta_x\eta_y\sigma_\delta^2] + Y^2[S_3^2\sigma_{x0}^2 + C_3^2\sigma_{y0}^2 - S_6\eta_x\eta_y\sigma_\delta^2] + XY[S_6(\sigma_{x0}^2 - \sigma_{y0}^2) - 2C_6\eta_x\eta_y\sigma_\delta^2]\} \tag{16}$$

$$\frac{\Delta\varepsilon_y}{\varepsilon_{y0}} = \frac{\beta_y}{2\varepsilon_{y0}} (K_2 L)^2 \{X^2[S_3^2\sigma_{x0}^2 + C_3^2\sigma_{y0}^2 - S_6\eta_x\eta_y\sigma_\delta^2] + Y^2[C_3^2\sigma_{x0}^2 + S_3^2\sigma_{y0}^2 + S_6\eta_x\eta_y\sigma_\delta^2] - XY[S_6(\sigma_{x0}^2 - \sigma_{y0}^2) - 2C_6\eta_x\eta_y\sigma_\delta^2]\} \tag{17}$$

$$\sigma_{x0}^2 = \beta_x\varepsilon_{x0} + \eta_x^2\sigma_\delta^2 ; \quad \sigma_{y0}^2 = \beta_y\varepsilon_{y0} + \eta_y^2\sigma_\delta^2 \tag{18}$$

$$S_3 = \sin(3\psi) ; \quad C_3 = \cos(3\psi) ; \quad S_6 = \sin(6\psi) ; \quad C_6 = \cos(6\psi) \tag{19}$$

For the case of normal sextupoles and horizontal dispersion only, the Eqs. (16) and (17) are reduced to the same result as in [1]:

$$\frac{\Delta\varepsilon_x}{\varepsilon_{x0}} = \frac{\beta_x}{2\varepsilon_{x0}}(K_2L)^2\{X^2\sigma_{x0}^2 + Y^2\sigma_{y0}^2\} = \frac{1}{2}\beta_x^2(K_2L)^2\left\{X^2\left(1+\frac{\eta_x^2\sigma_\delta^2}{\beta_x\varepsilon_{x0}}\right) + Y^2\frac{\beta_y\varepsilon_{y0}}{\beta_x\varepsilon_{x0}}\right\} \quad (20)$$

$$\frac{\Delta\varepsilon_y}{\varepsilon_{y0}} = \frac{\beta_y}{2\varepsilon_{y0}}(K_2L)^2\{X^2\sigma_{y0}^2 + Y^2\sigma_{x0}^2\} = \frac{1}{2}\beta_x\beta_y\left(\frac{\varepsilon_{x0}}{\varepsilon_{y0}}\right)(K_2L)^2\left\{X^2\frac{\beta_y\varepsilon_{y0}}{\beta_x\varepsilon_{x0}} + Y^2\left(1+\frac{\eta_x^2\sigma_\delta^2}{\beta_x\varepsilon_{x0}}\right)\right\} \quad (21)$$

6 References

[1] P. Emma and M. Venturini, "Emittance Dilution in Linac-Based Free-Electron Lasers," unpublished, 2017.

[2] H. Grote and F. C. Iselin, "The MAD Program," http://mad8.web.cern.ch/mad8/.

[3] M. Borland, "elegant: A Flexible SDDS-Compliant Code for Accelerator Simulation," Advanced Photon Source LS-287, September 2000.

[4] M. Woodley, "LCLS-II-HE Lattice," https://www.slac.stanford.edu/grp/ad/model/lcls2he.html.

[5] J. Qiang, private communication.